THE JOURNAL OF BIOLOGICAL CHEMISTRY VOL. 290, NO. 3, pp. 1689–1698, January 16, 2015

Experimental Evidence for a Hydride Transfer Mechanism in Plant Glycolate Oxidase Catalysis*

Received for publication, October 13, 2014, and in revised form, November 21, 2014 Published, JBC Papers in Press, November 21, 2014, DOI 10.1074/jbc.M114.618629

Younès Dellero[‡1], Caroline Mauve[‡§], Edouard Boex-Fontvieille[‡], Valérie Flesch[‡], Mathieu Jossier[‡], Guillaume Tcherkez[‡§¶], and Michael Hodges[‡2]

From the [‡]Institut de Biologie des Plantes, CNRS UMR8618, Saclay Plant Sciences, Bâtiment 630, Université Paris Sud, 91405 Orsay Cedex, France, [§]Plateforme Métabolisme-Métabolome, Saclay Plant Sciences, Institut de Biologie des Plantes, Bâtiment 630, 91405 Orsay Cedex, France, and [¶]Institut Universitaire de France, 103 Boulevard Saint-Michel, 75005 Paris, France

Background: Uncertainty remains about the nature of transition states along the reductive half-reaction of glycolate oxidase.
Results: Deuterated glycolate and solvent slow down plant glycolate oxidase catalysis to a modest extent.
Conclusion: Isotope effects support a hydride transfer mechanism and indicate glycolate deprotonation to be only partially rate-limiting.
Significance: Understanding the catalytic mechanism of the enzyme is crucial for designing drugs/herbicides to inhibit its activity.

In plants, glycolate oxidase is involved in the photorespiratory cycle, one of the major fluxes at the global scale. To clarify both the nature of the mechanism and possible differences in glycolate oxidase enzyme chemistry from C_3 and C_4 plant species, we analyzed kinetic parameters of purified recombinant C_3 (*Arabidopsis thaliana*) and C_4 (*Zea mays*) plant enzymes and compared isotope effects using natural and deuterated glycolate in either natural or deuterated solvent. The $^{12}C/^{13}C$ isotope effect was also investigated for each plant glycolate oxidase protein by measuring the ^{13}C natural abundance in glycolate using natural or deuterated glycolate as a substrate. Our results suggest that several elemental steps were associated with an hydrogen/deuterium isotope effect and that glycolate α-deprotonation itself was only partially rate-limiting. Calculations of commitment factors from observed kinetic isotope effect values support a hydride transfer mechanism. No significant differences were seen between C_3 and C_4 enzymes.

Glycolate oxidase (EC 1.1.3.15; glycolate:oxygen oxidoreductase; GOX[3]) is a peroxisomal enzyme that converts glycolate into glyoxylate with the production of hydrogen peroxide from O_2 via a flavin mononucleotide (FMN)-mediated reaction. This enzyme is a member of the α-hydroxy-acid oxidase superfamily, which includes short-chain and long-chain hydroxy-acid oxidases, lactate oxidase, and the flavin-binding domain of yeast flavocytochrome b_2 (1). It appears that plant and animal GOXs (short-chain α-hydroxy-acid oxidases) arose from a common eukaryotic GOX ancestor that originated from a bacterial lactate oxidase (2). In mammals, GOX is responsible for the production of oxalate (3), and therefore it is a potential site for therapeutic agents to treat primary hyperoxaluria (4), a genetic disorder that leads to large kidney stones due to calcium oxalate deposition. In plants, GOX is involved in the photorespiratory cycle, a metabolic pathway that recycles phosphoglycolate from ribulose-1,5-bisphosphate carboxylase/oxygenase (EC 4.1.1.39) (Rubisco)-catalyzed oxygenation. Photorespiratory glycolate oxidation by terrestrial vegetation represents a flux of nearly 3 Pmol/year and is thus one of the major fluxes at the global scale (5).

To date, the best characterized GOX in terms of structure, kinetics, and biochemical properties is from spinach leaves (*Spinacia oleracea*). The three-dimensional structure of spinach GOX has identified Ser^{106}, Tyr^{129}, Thr^{155}, and Lys^{230} as important residues in the stabilization of the FMN cofactor, whereas Tyr^{24}, Tyr^{129}, and Arg^{257} are involved in substrate binding. His^{254} is essential for catalysis as it is involved in the proton abstraction from the glycolate C2 atom (6). This role was found in other α-hydroxy-acid oxidase superfamily members because mutation of the equivalent His residue (H373Q for flavocytochrome b_2 and H290Q for lactate oxidase) led to reduced activities and substrate K_m values or inactive recombinant proteins (7, 8). The recent structure of human liver GOX has indicated the conservation of the active site residues between plant and animal enzymes (9). A ping-pong bi-bi reaction mechanism composed of two half-reactions has been proposed for GOX. In the reductive half-reaction, after the reversible formation of the Michaelis complex between the enzyme and glycolate, protons are abstracted from glycolate C2 and accepted by the FMN (Fig. 1). The complex is then dissociated, and glyoxylate is released. Stopped-flow studies using recombinant GOX produced in bakers' yeast (*Saccharomyces cerevisiae*) suggested the FMN reduction step of GOX catalysis to be rate-limiting (10). In the oxidative half-reaction, FMN is reoxidized by O_2 to produce hydrogen per-

* This work was supported in part by French State Grants ANR-10-LABX-0040-SPS (managed by the French National Research Agency under the Investments for the Future Program ANR-11-IDEX-0003-02) and ANR JC 12-0001-01 (to G. T.), the CNRS, and the Université Paris Sud.
[1] Supported by a Ph.D. grant from the French Ministry of Higher Education and Research.
[2] To whom correspondence should be addressed. Tel.: 33-169153335; Fax: 33-169153424; E-mail: michael.hodges@u-psud.fr.
[3] The abbreviations used are: GOX, glycolate oxidase; Rubisco, ribulose-1,5-bisphosphate carboxylase/oxygenase; KIE, kinetic isotope effect; SIE, solvent isotope effect.

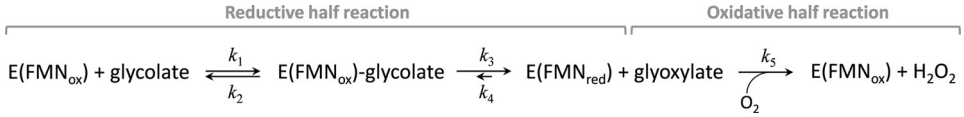

FIGURE 1. **Formal mechanism of the GOX-catalyzed reaction.** In the reductive half-reaction, after the formation of the Michaelis complex GOX-glycolate, protons are abstracted from glycolate and accepted by the FMN. The enzyme-substrate complex is dissociated, and glyoxylate is released. In the oxidative half-reaction, FMN is reoxidized by O_2 to produce hydrogen peroxide. The notation for rate constants (k_1, k_2, k_3, k_4, and k_5) follows that of Macheroux *et al.* (10).

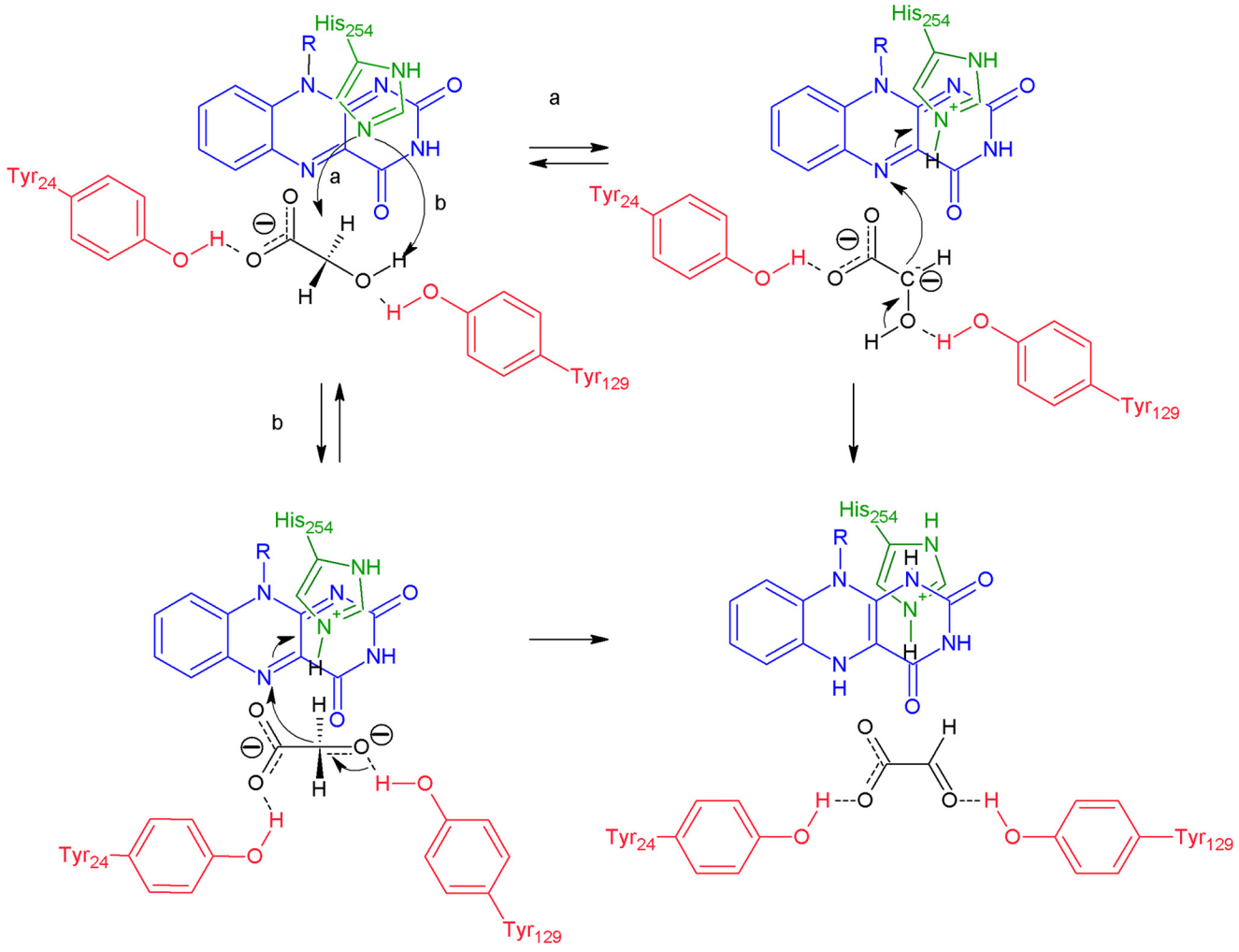

FIGURE 2. **Possible mechanisms of glycolate deprotonation catalyzed by GOX.** *a*, carbanion-based stepwise mechanism. *b*, concerted hydride transfer. The interactions within the active site between glycolate (*black*), Tyr^{24} and Tyr^{129} (*red*), His^{254} (*green*), and the isoalloxazine ring of FMN (*blue*) are shown, and additional interactions with other residues are omitted for clarity. Note that the two mechanisms presented differ by the nature of the first proton being attacked by His^{254}. In *b*, proton abstraction from O2 (hydroxyl) and C2 (α-proton) are shown as two separate steps, but they may occur within the same reaction elemental step (asynchronous concerted rearrangement).

oxide. Recently, new spectroscopy advances have been used to indicate that reduced FMN undergoes a two-step oxidation in recombinant human liver GOX (11).

Despite the current knowledge of the chemical basis of GOX catalysis, uncertainty remains about the nature of transition states along the reductive half-reaction. Two scenarios (see Fig. 2) are described in the literature that differ by the position of the first abstracted proton and thus the sequence of elemental steps. In the carbanion-based mechanism (Fig. 2*a*), the side chain of a crucial histidine residue (His^{254} in spinach GOX) abstracts the α-proton from the C2 atom of glycolate, leading to the formation of a negatively charged intermediate. The proton of the hydroxyl group attached to the C2 atom of glycolate is then abstracted by the N5 of the FMN. In the hydride transfer mechanism (Fig. 2*b*), the two protons are abstracted in a concerted manner with the side chain of the His residue abstracting the proton of the hydroxyl group of glycolate, and at the same time, the α-proton is transferred to the N5 atom of the FMN (see Ref. 12). Interestingly, previous studies have shown differences between the kinetic parameters of GOXs from C_3 and C_4 plant species. GOX from C_4 species appear to have a lower K_m for glycolate (10 μM for *Amaranthus hypochondriacus* and 23 and 65 μM for *Zea mays* guard cells and mesophyll cells, respectively) compared with C_3 species (330 μM for *Cucurbita pepo* cotyledons, 300 μM for *Pisum sativum*, 1 mM for *S. oleracea*, and 1.9 mM for *Arabidopsis thaliana* GOX2) (13–16). These obser-

vations suggest potential differences in substrate binding and perhaps reaction velocity kinetics. Such differences would correspond to an adaptation to cellular metabolic conditions, that is the naturally lower glycolate contents in C_4 plants due to the reduced photorespiration. Furthermore, it might be hypothesized that the enzyme from C_3 species would have a larger V_{max} to ensure maximal glycolate conversion at high photorespiratory rates. However, there is presently little data that compare the catalytic effectiveness of C_3 and C_4 enzymes, including the determination of limiting steps.

As an aid in clarifying both the nature of the mechanism and possible differences in C_3 and C_4 enzyme chemistry, we analyzed the kinetics of recombinant C_3 and C_4 enzymes using isotope effects. Kinetic parameters of purified recombinant GOX1 (At3g14420) and GOX2 (At3g14415) from *A. thaliana* (the two GOX genes highly expressed in leaves) and GO1 from *Z. mays* (the gene giving a photorespiratory phenotype when mutated (17)) were compared using natural and deuterated glycolate in either natural or deuterated solvent. The $^{12}C/^{13}C$ isotope effect was also investigated for each plant GOX protein by measuring the ^{13}C natural abundance in glycolate using natural or deuterated glycolate as a substrate. Our results suggest that several elemental steps are associated with an hydrogen/deuterium isotope effect and that glycolate α-deprotonation itself is only partially rate-limiting. Calculations of commitment factors from observed kinetic isotope effect (KIE) values support a hydride transfer mechanism. No significant differences were seen between C_3 and C_4 enzymes.

EXPERIMENTAL PROCEDURES

Constructs to Express Plant GOX Proteins in Escherichia coli Cells—The coding regions of AtGOX1 and ZmGO1 were PCR-amplified using different cDNA templates, gene-specific primers with added restriction enzyme sites (AtGOX1-NheI and AtGOX1-XhoI; ZmGO1-NheI and ZmGO1-XhoI), and *Taq* polymerase (Promega). Total RNA was extracted from *A. thaliana* rosette leaves using TRIzol® as in Jossier *et al.* (18). All other DNA manipulations such as plasmid isolation, *E. coli* transformation, ligations, and restriction analyses were standard techniques. The template for *Arabidopsis* GOX1 was a cDNA made from reverse transcribed RQ1 DNase-treated total RNA from rosette leaves using AtGOX1-F and AtGOX1-R primers. The template for *Z. mays* GO1 was a full-length cDNA ordered from Arizona Genomics Institute (clone ZM_BFc0135O12). The templates were diluted and used for PCR amplification. The gene-specific primers were as follows: AtGOX1-NheI, CGGCTAGCGAGATCACTAACGTTACCG; AtGOX1-XhoI, GGGCTCGAGCTATAACCTGGCTGAAGGAC; ZmGO1-NheI, CGGCTAGCGGGGAGATCACCAATGTCATG; ZmGO1-Xho1, GGGCTCGAGCTACAAGCGCGACGGGATG; AtGOX1-F, ACACTTCGGCATATGGAGATCACTAACGTT; and AtGOX1-R, ATTTTCCCTCGAGTAACCTGGCTGAAGGACG.

Each PCR-amplified product was purified using a PCR CleanUp kit (Macherey-Nagel), cloned into the pGEMT easy vector (Promega), and sequenced (MWG Operon, Eurofins). The verified coding sequences were transferred to the pET28a expression vector (Novagen) after digestion with NheI and XhoI restriction enzymes (Promega) and overnight ligation. All final constructs were verified by restriction analyses using purified plasmids from isolated bacterial colonies. The construct pET28a-AtGOX2 was a kind gift from Hägemann and co-workers (16). The recombinant pET28a vectors (pET28a-AtGOX1, pET28a-AtGOX2, and pET28a-ZmGO1) were used to transform *E. coli* strain BL21(DE3) by electroporation.

Purification of Recombinant GOX—E. coli BL21 cells containing pET28a-AtGOX1, pET28a-AtGOX2, or pET28a-ZmGO1 were grown in 200 ml of Luria-Bertani broth to an $A_{600\,nm}$ of 0.4 at 37 °C. GOX protein expression was induced by addition of 1 mM isopropyl β-1-D-thiogalactopyranoside for 20 h at 30 °C. GOX proteins were purified via their N-terminal His tag using His-Select nickel affinity resin (Sigma-Aldrich) according to Hackenberg *et al.* (16) with some modifications. Cells were harvested and resuspended in resuspension buffer consisting of 50 mM Tris-HCl, pH 8.0 containing 1 M NaCl, 10 mM imidazole, 10% glycerol, 0.1 mM FMN, and a protease inhibitor mixture (Complete Mini, EDTA-free, Roche Applied Science) on ice. Bacterial cells were broken by three passages through a French press at 600 pascals. After centrifugation (15,500 × *g* for 30 min at 4 °C), soluble proteins were diluted to 10 ml and incubated with continual mixing for 3 h with 1.5 ml of affinity resin at 4 °C. The resin was washed with 50 ml of resuspension buffer supplemented with 20 mM imidazole. His-tagged GOX proteins were then eluted using resuspension buffer supplemented with 250 mM imidazole. The first 0.5-ml elution fraction was disregarded because it did not contain recombinant protein, and the next 2.5 ml of 0.5-ml fractions was pooled to give the soluble GOX fraction that was immediately desalted through PD-10 columns (GE Healthcare) equilibrated with 50 mM Tris-HCl, pH 8.0, 20% glycerol, and 0.1 mM FMN following the manufacturer's instructions. The purity of each recombinant GOX protein was checked by SDS-PAGE (12% acrylamide) stained with Coomassie Brilliant Blue (19). Protein concentration was determined using the Bradford reagent (Sigma-Aldrich) according to the manufacturer's instructions. Purified GOX was stored at 4 °C for up to 7 days without any modification in enzymatic activity. For isotopic discrimination experiments, GOX was purified as described above except that desalting was carried out in the absence of glycerol because it interfered with the HPLC separation of glycolate.

GOX Activity Measurements—Enzyme activity was measured in 50 mM Tris-HCl, pH 8.0 with different glycolate concentrations (0.1–10 mM) and 4 μg of purified recombinant GOX by an enzyme-coupled reaction at 30 °C. Glycolate-dependent H_2O_2 production was quantified in the presence of 0.4 mM *o*-dianisidine and 2 units of horseradish peroxidase by measuring the $\Delta A_{440\,nm}$ using a Varian Cary 50 spectrophotometer. GOX activity assays with stable isotopes were performed using deuterium oxide (99.9 atom % D; Sigma-Aldrich), deuterium chloride (solution 35% (w/w) in D_2O, 99.9 atom % D; CDN Isotopes), 2,2-d_2-glycolic acid (99.6 atom % D; CDN Isotopes). For enzyme activity measurements in heavy water (D_2O), all reaction components were dissolved in D_2O except for the purified recombinant GOX. In this way, the reaction mixture contained at least 95% D_2O. Measurements were performed at pD 8, stabilized by the addition of deuterium chlo-

ride, and supplemented with 10 units of horseradish peroxidase (as this enzyme was affected by D_2O) such that H_2O_2 conversion was always quantitative and not influenced by deuteration. Kinetic parameters were calculated by fitting the data to different equations (see "Enzyme Kinetics" below).

HPLC Purification of Glycolate and Isotopic Measurements—Five micrograms of purified recombinant GOX protein was mixed with 1 mM natural glycolate or deuterated glycolate in 50 mM Tris-HCl, pH 8.0 or with 200 μM natural glycolate or deuterated glycolate in 10 mM Tris-HCl, pH 8.0, and the reaction was quenched at different times by adding 1 M HCl. Samples were lyophilized and resuspended in 100 μl of distilled water. 50 μl of the resulting solution was injected for HPLC (LC-1260, Agilent Technologies). Tris, glycolate, and glyoxylate were separated by anion exchange (RS Pak KC-811, Shodex) at 30 °C with isocratic degassed water as the mobile phase (flow rate, 0.5 ml min^{-1}). Detection was performed using a refractometer at 35 °C. Glycolate amounts were determined after HPLC separation using a standard curve. The $^{13}C/^{12}C$ ratio in glycolate was measured as follows. HPLC-separated compounds were desolvated and converted to CO_2 on line by chemical oxidation (by 15% ammonium persulfate and 5% orthophosphoric acid) using a specific interface (Liquiface, Elementar), and resulting CO_2 molecules entered the isotope ratio mass spectrometer (Isoprime, Elementar) under continuous flow mode (with helium as carrier gas). A Nafion® membrane placed within the interface was used to remove water generated by chemical oxidation. $\delta^{13}C$ values were expressed relative to the standard Vienna Pee Dee Belemnite in ‰. $\delta^{13}C$ values were calibrated using sucrose (Sigma-Aldrich) as a standard, and the $\delta^{13}C$ value of commercial glycolate and sucrose was checked by elemental analysis coupled to isotope ratio mass spectrometry (Pyrocube-Isoprime 100, Elementar). The $\delta^{13}C$ value was further corrected to account for concentration (isotopic non-linearity) effect using a response curve of $\delta^{13}C$ in commercial glycolate to glycolate concentration. Such a correction was nevertheless always very small (<0.2‰), and it did not affect results to a significant extent.

Enzyme Kinetics—The reaction scheme depicted in Fig. 1 gives the following expression of velocity (10).

$$v = \frac{V_{max}}{1 + K_m/S + K_o/O} \qquad \text{(Eq. 1)}$$

where $V_{max} = k_3[E_0]$ is maximal velocity at saturating glycolate, and S and O are glycolate and dissolved oxygen (O_2) concentrations, respectively. Michaelis constants for glycolate (K_m) and oxygen (K_o) are given by Equation 2.

$$K_m = \frac{k_2 + k_3}{k_1}; \quad K_o = \frac{k_3}{k_5} \qquad \text{(Eq. 2)}$$

The apparent maximal velocity and Michaelis constant for glycolate (denoted as V_{max}^{app} and K_m^{app}, respectively) stand for kinetic parameters when reaction kinetics are fitted to a simple (non O_2-dependent) Michaelis expression, *i.e.* $v = V_{max}^{app}S/(K_m^{app} + S)$. V_{max}^{app} and K_m^{app} were simply obtained using a classical hyperbolic fit of experimental curves using SigmaPlot (Systat Software Inc.). Actual kinetic parameters ($k_{cat} = k_3$, K_m, and K_o) were obtained by step-by-step fitting of experimental data, *i.e.* by performing multiple hyperbolic fitting at fixed k_{cat} values and choosing the best set of kinetic parameters that minimized the sum of squares (residuals). Solving simultaneously all parameters by numeric optimization of the linearized equation.

$$\ln v = \ln V_{max} + \ln\left(1 + \frac{K_m}{S} + \frac{K_o}{O}\right) \qquad \text{(Eq. 3)}$$

with the Excel solver software (Microsoft) yielded the same results. The knowledge of k_3 allows the calculation of k_2 because the commitment factor $c = k_3/k_2$ is determined using isotope effects (see below), and therefore k_1 and k_5 can be determined using Equation 2.

Isotope Effects—$^1H/^2H$ isotope effects were calculated using the ratio of kinetic parameters (described below) obtained with either the natural or the deuterated substrate/solvent. $^{12}C/^{13}C$ isotope effects were calculated from the time course of the $^{13}C/^{12}C$ ratio in glycolate using the Rayleigh relationship.

$$\alpha = \frac{\ln(1-f)}{\ln(1-f) + \ln\left(\frac{R_t}{R_0}\right)} \qquad \text{(Eq. 4)}$$

where f is the fraction of consumed glycolate, R_0 is the $^{13}C/^{12}C$ ratio of glycolate at $t = 0$ (before the reaction commenced), and R_t is the $^{13}C/^{12}C$ ratio of glycolate at time t. f was determined using glycolate quantitation by HPLC (the same result was obtained with the mass 44 signal on the isotope ratio mass spectrometer. The observed KIE on the effective reaction rate is denoted as $\alpha_{V/K}$ and is given by Equation 5.

$$\alpha_{v/K} = {}^{l}\left(\frac{k_3}{K_m}\right) \Big/ {}^{h}\left(\frac{k_3}{K_m}\right) = \alpha_1 \frac{\alpha_3 + \frac{k_3}{k_2} \cdot \frac{1}{\alpha_2}}{1 + \frac{k_3}{k_2}} \qquad \text{(Eq. 5)}$$

where l is light and h is heavy substrate. The KIE on maximal velocity is given by Equation 6.

$$\alpha_V = {}^{light}k_3/{}^{heavy}k_3 \qquad \text{(Eq. 6)}$$

The kinetic isotope effect on apparent turnover (V_{max}^{app}) is given by Equation 7.

$$\alpha_V^{app} = \frac{\alpha_3 + \alpha_5 \frac{K_o}{O}}{1 + \frac{K_o}{O}} \qquad \text{(Eq. 7)}$$

where α_i is the intrinsic isotope effects associated with k_i ($= {}^{light}k_i/{}^{heavy}k_i$), and thus, $\alpha_3 = \alpha_V$. In what follows, superscripts "13" and "D" attached to the symbol α refer to $^{12}C/^{13}C$ and $^1H/^2H$ isotope effects, respectively. It should be noted that in the case of ^{13}C there is no isotope effect on k_1 and k_2 (no bond cleavage or formation with the carbon atom), and therefore Equation 5 simplifies to Equation 8.

$$^{13}\alpha_{V/K} = \frac{^{13}\alpha_3 + \frac{k_3}{k_2}}{1 + \frac{k_3}{k_2}} \quad \text{(Eq. 8)}$$

Because the $^{12}C/^{13}C$ KIE on maximal velocity, $^{13}\alpha_3$, is determined experimentally (Equation 5), the commitment factor $c = k_3/k_2$ can be calculated using either natural or deuterated glycolate. Using the obvious relationship $^{H}c/^{D}c = {}^{D}\alpha_3/{}^{D}\alpha_2$, $^{D}\alpha_2$ can thus be calculated as $^{D}\alpha_3/(^{H}c/^{D}c)$. Therefore, $^{D}\alpha_1$ can be computed using Equation 5. α_5 is obtained using Equation 7.

RESULTS

Steady-state Kinetic Parameters of Recombinant AtGOX1, AtGOX2, and ZmGO1—Arabidopsis GOX1 and GOX2 (C_3 plant) and *Z. mays* GO1 (C_4 plant) were expressed as N-terminal His-tagged proteins in *E. coli*. His-GOX proteins were purified by affinity chromatography (Fig. 3), and their identity was confirmed by mass spectrometry (data not shown). The presence of higher molecular mass proteins was occasionally observed (as seen in Fig. 3); however, it should be noted that their presence did not modify the measured kinetic parameters. For each GOX tested, their catalytic activities were measured over a range of glycolate concentrations (0.1–10 mM) at around 0.2 mM O_2. Apparent turnover rate k_{cat}^{app} (k_3^{app}) and Michaelis constant K_m^{app} values were calculated by fitting to ordinary Michaelis-Menten kinetics: $v = V_{max}^{app}/(1 + K_m^{app}/S)$. K_m and K_o/O were calculated by numerical resolution (see "Experimental Procedures") (Table 1) to fit the formal equation (Equation 1). There were no significant differences in the fitted kinetic parameters between GOXs from C_3 and C_4 species with natural glycolate as a substrate (Table 1). Our different GOX proteins exhibited k_{cat} (k_3) values from 30 to 34 s^{-1} and K_m values from 0.22 to 0.30 mM as reported for recombinant GOX enzymes from plants and animals examined so far (10, 11, 13, 14, 20, 21). The K_o/O value we found (≈0.15) was also comparable with that of spinach GOX (0.5 in Ref. 22). With deuterated glycolate as a substrate, k_{cat}^{app} and k_{cat} decreased 2–3-fold, and both K_m^{app} and K_m increased 1.5–2-fold. By contrast, the effect of changing the solvent to D_2O was visible but not large with a solvent isotope effect (SIE) value of about 1.5 on k_{cat} (see also below). The SIE was always smaller and thus close to unity on catalytic effectiveness (V/K) regardless of the GOX isoform considered.

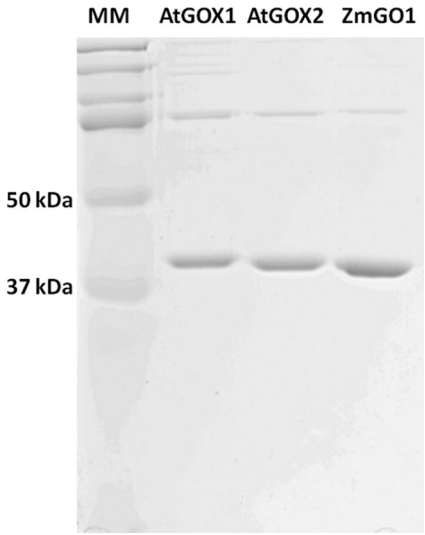

FIGURE 3. **Purity of each recombinant GOX.** Two micrograms of desalted purified GOX protein was separated by SDS-PAGE (12% acrylamide) and stained with Coomassie Blue. The expected molecular mass (*MM*) for each monomeric GOX is ~40 kDa.

Hydrogen/Deuterium and $^{13}C/^{12}C$ KIE of Recombinant AtGOX1, AtGOX2, and ZmGO1—The observed KIE and SIE values calculated from kinetic parameters (Table 1) are listed in Table 2. We found a KIE on turnover, $^{D}\alpha_V$, of about 2 and a KIE on catalytic effectiveness, $^{D}\alpha_{V/K}$, of about 4 for each of the three GOX enzymes. All of these KIE values are significantly different from unity ($p < 0.05$). In other words, the KIE on the turnover rate was larger than that on catalytic effectiveness, suggesting that catalytic steps prior to glycolate deprotonation itself (k_3) were associated with a KIE (rate constants k_1 and k_2; Fig. 1). The

TABLE 1

Steady-state kinetic parameters of recombinant GOX enzymes assayed with either [^{1}H]glycolate (H), [^{2}H]glycolate (D), or D_2O as a solvent

GOX activity was measured by following the formation of the *o*-dianisidine radical by spectrometry ($\Delta A_{440\,nm}$) at 30 °C and pH 8. Kinetic parameters were calculated by fitting the data to Equation 1 or using a simple Michaelis model (superscript "app") (see "Experimental Procedures"). Values represent the mean ± S.D. from three independent enzyme preparations for each GOX tested. Parameters in bold are significantly different compared with the control experiment (H) ($p < 0.05$).

	H		D		D_2O	
Conditions	**Mean**	**S.D.**	**Mean**	**S.D.**	**Mean**	**S.D.**
AtGOX1						
k_3 (s^{-1})	29.86	2.84	**14.93**	0.71	**24.41**	2.96
K_m (mM)	0.22	0.03	**0.36**	0.02	0.20	0.02
K_o/O	0.17	0.12	0.33	0.07	0.25	0.13
k_3^{app} (s^{-1})	26.57	4.90	**12.35**[a]	0.61	20.11	3.39
K_m^{app} (mM)	0.20	0.07	**0.34**	0.08	0.17	0.04
AtGOX2						
k_3 (s^{-1})	30.10	6.37	**12.80**	4.32	**20.14**	2.17
K_m (mM)	0.30	0.09	**0.57**[a]	0.10	0.27	0.10
K_o/O	0.23	0.14	0.29	0.19	0.24	0.09
k_3^{app} (s^{-1})	25.07	3.03	**10.17**	1.25	**17.92**	2.55
K_m^{app} (mM)	0.22	0.03	**0.44**[a]	0.14	0.23	0.07
ZmGO1						
k_3 (s^{-1})	34.13	3.25	**12.56**	1.48	**21.57**	2.49
K_m (mM)	0.22	0.06	**0.33**	0.03	0.13	0.05
K_o/O	0.16	0.12	0.21	0.02	0.17	0.08
k_3^{app} (s^{-1})	28.16	2.94	**9.90**	0.91	**19.25**	2.87
K_m^{app} (mM)	0.17	0.04	**0.24**	0.01	0.13	0.05

[a] Significantly different from other enzymes ($p < 0.05$).

TABLE 2

$^{1}H/^{2}H$ KIE (associated with deuterated glycolate) and solvent isotope effect (D_2O) on GOX catalysis

Values represent the mean ± S.D. from three independent enzyme preparations for each GOX tested. Parameters shown in bold are significantly different from unity (*i.e.* no KIE) ($p < 0.05$).

	Mean	S.D.
AtGOX1		
$^{D}\alpha_{V}^{app}$	**2.14**	0.32
$^{D}\alpha_{V}$	**2.00**	0.17
$^{D}\alpha_{V/K}^{app}$	**3.65**	0.89
$^{D}\alpha_{V/K}$	**3.35**	0.34
$^{D2O}\alpha_{V}$	**1.23**	0.05
$^{D2O}\alpha_{V/K}$	1.17	0.26
$^{D}\alpha_{Ko/O}$	**0.48**	0.25
AtGOX2		
$^{D}\alpha_{V}^{app}$	**2.46**	0.01
$^{D}\alpha_{V}$	**2.46**	0.68
$^{D}\alpha_{V/K}^{app}$	**4.80**	1.02
$^{D}\alpha_{V/K}$	**4.67**	0.62
$^{D2O}\alpha_{V}$	**1.48**	0.18
$^{D2O}\alpha_{V/K}$	1.31	0.33
$^{D}\alpha_{Ko/O}$	1.34	1.62
ZmGO1		
$^{D}\alpha_{V}^{app}$	**2.84**	0.05
$^{D}\alpha_{V}$	**2.72**	0.14
$^{D}\alpha_{V/K}^{app}$	**4.16**	1.10
$^{D}\alpha_{V/K}$	**4.19**	0.93
$^{D2O}\alpha_{V}$	**1.59**	0.05
$^{D2O}\alpha_{V/K}$	0.92	0.14
$^{D}\alpha_{Ko/O}$	0.77	0.55

TABLE 3

$^{12}C/^{13}C$ isotope effect in GOX catalysis with either natural or deuterated glycolate

The $^{13}C/^{12}C$ isotopic effect was calculated using $\delta^{13}C$ values (natural abundance) and glycolate concentrations (see "Experimental Procedures"). Values presented are mean ± S.D. for three replicate experiments for each GOX enzyme. Parameters shown in bold are significantly different from unity ($p < 0.05$).

	AtGOX1	AtGOX2	ZmGO1
$^{13}\alpha_{V}$	**1.0440 ± 0.0011**	**1.0454 ± 0.0094**	**1.0428 ± 0.0059**
$^{13}\alpha_{V/K}$	**1.0193 ± 0.0042**	**1.0194 ± 0.0031**	**1.0195 ± 0.0026**
$^{13}{}^{D}\alpha_{V}$	**1.0951 ± 0.01133**	**1.0911 ± 0.0133**	**1.0996 ± 0.0141**
$^{13}{}^{D}\alpha_{V/K}$	**1.0463 ± 0.0084**	**1.0423 ± 0.0093**	**1.0468 ± 0.0085**

$^{D}\alpha_{Ko/O}$ is less than unity in AtGOX1, but it is close to unity in AtGOX2 and ZmGO1. It should nevertheless be noted that there is a quite large uncertainty (standard error) in $^{D}\alpha_{Ko/O}$. If $^{D}\alpha_{Ko/O}$ were effectively not different from unity, then this would mean that the rate constant associated with FMN oxidation (H_2O_2 production) would be associated with a KIE, thereby compensating for the KIE on k_3 (Equation 7; see also "Discussion"). The SIE on turnover, $^{D2O}\alpha_{V}$, was within the range of 1.2–1.6 for all three GOX enzymes and was significantly different from unity ($p < 0.05$). The rather modest SIE suggests that within the active site exchangeable protons were not primarily involved in proton abstraction from glycolate but rather involved in weak bonds (secondary isotope effect) in the active site. Interestingly, $D_2O\alpha_{V/K}$ values were always very close to unity, suggesting that D_2O also affected steps prior to proton abstraction (k_2 and k_1) so that substrate binding appeared to be tighter in heavy water.

The $^{13}C/^{12}C$ KIE in the GOX reaction for all three enzymes is shown in Table 3. The carbon isotope composition of glycolate ($\delta^{13}C$) was determined at different experimental times along the reaction by acid quenching followed by HPLC-co-isotope ratio mass spectrometry. The $^{13}C/^{12}C$ KIE was calculated with Equation 6 (Rayleigh's equation) and recalculated (fractionation $\alpha - 1$ multiplied by a factor 2) to convert to a positional isotope effect (rather than a molecular average-based isotope effect). In other words, we assumed here that only one carbon atom position (C2) in glycolate was responsible for the $^{12}C/^{13}C$ KIE and that the secondary KIE on the C1 atom position was negligible. We thus found a KIE value on the turnover rate $^{13}\alpha_{V}$ of around 1.045 and a value on the catalytic effectiveness $^{13}\alpha_{V/K}$ of around 1.019 for all three enzymes (Table 3). The fact that the KIE on *V/K* (effectiveness) was smaller than that on *V* (turnover) suggests that deprotonation (k_3) was partially rate-limiting. Quite remarkably, $^{12}C/^{13}C$ KIEs (both $^{13}\alpha_{V}$ and $^{13}\alpha_{V/K}$) increased (the fractionation was doubled) when deuterated glycolate was used as a substrate, suggesting that the $^{13}C/^{12}C$ KIE originated from chemical events associated with glycolate deprotonation.

DISCUSSION

Recombinant GOX from C_3 and C_4 Plant Species Share Similar Kinetic Properties—Previous studies have shown the K_m for glycolate of leaf-purified GOX of C_3 species to be higher than that of C_4 species (see the Introduction). This could reflect the low photorespiratory activity in C_4 species as compared with C_3 species and therefore the requirement of a lower K_m for glycolate to allow a sufficient GOX activity in C_4 species. In this work, recombinant His-tagged GOX enzymes from *A. thaliana* (C_3 species) and *Z. mays* (C_4 species) were compared (Table 1). The obtained kinetic parameters agreed with previous $K_{m(glycolate)}$ values from plant-purified GOXs (0.3 mM in pumpkin cotyledons (13) and *P. sativum* leaves (14)) and recombinant mammalian GOX (0.32 mM in human (20)). Our different plant GOX proteins also exhibited k_{cat} values similar to those found in the literature (27 s^{-1} for purified pumpkin cotyledon GOX (14), 20 s^{-1} for recombinant spinach GOX (10), and 15.6 and 24 s^{-1} for purified and recombinant human liver GOXs (11, 21). Therefore, our GOX proteins appear to be fully functional. It is possible that the differences in K_m values reported in the literature arise from differing degrees of protein purity, the method used to purify each protein, and/or the presence or absence of heteromeric GOX protein complexes. However, it is also possible that they reflect a differential post-translational modification occurring only in plant-purified GOX proteins from C_3 and C_4 plant species. To date, two post-translational modifications for GOX proteins have been reported: nitrosylation (which inhibits GOX activity (23)) and phosphorylation (see Ref. 24 and the PhosPhAt database). In fact, the recombinant proteins used in this work were found to be neither phosphorylated nor nitrosylated (using mass spectrometry; data not shown).

Does GOX Catalysis Follow a Hydride Transfer Mechanism?—Two scenarios (see the Introduction and Fig. 2) have been described in the literature to describe the catalytic mechanism of α-hydroxy-acid oxidase family members: a mechanism involving a carbanion (stepwise mechanism) and a hydride transfer (concerted but maybe asynchronous mechanism). Structural data of *Aerococcus viridians* lactate oxidase led to the proposal of a hydride transfer mechanism (25). With the recent advances in the use of stable isotopes (^{15}N, ^{13}C, and ^{2}H), the measurement of KIEs in bond cleavage have also provided evidence mostly in favor of a concerted hydride transfer in flavoprotein catalysis (26). The $^{14}N/^{15}N$ isotope effects associated

with Ser oxidation by D-amino-acid oxidase, sarcosine oxidation by *N*-methyltryptophan oxidase, and alanine oxidation by tryptophan 2-monooxygenase suggested a concerted proton abstraction mechanism for these reactions (27–29). In the case of serine oxidation by D-amino-acid oxidase, there is a KIE (corrected for the isotope effect of deprotonation of -NH_3^+) of 0.996 (*i.e.* 4‰ against ^{14}N), consistent with the production of a $C{=}NH_2^+$ intermediate rather than a carbanion ($C^-{-}NH_2$) (27). Similarly, a hydride transfer mechanism has been demonstrated in tryptophan 2-monooxygenase (28). In flavocytochrome b_2 (an α-hydroxy-acid oxidase family member), the modest isotope effect with [^{2}H]lactate suggested that substrate deprotonation was only partially rate-limiting, which is not strictly compatible with a carbanion-based mechanism. However, the fact that there was no solvent isotope effect (H_2O/D_2O) on flavin reduction suggested that cleavage of the O–H bond was not a critical chemical event to initiate the reaction, that is is probably not required for C–H bond cleavage, thereby suggesting that a carbanion intermediate was plausible (30). With that said, the hydride transfer mechanism was given further support by the characterization of the Tyr-to-Phe mutant, which exhibited both a large KIE (with [^{2}H]lactate) and a significant solvent isotope effect, demonstrating the interdependence of C–H and O–H cleavage (34). Therefore, we find arguments for and against a hydride transfer mechanism in flavoprotein oxidases, and critically, no specific studies had been carried out using GOX as an enzyme model. Previous works have suggested the reductive half-reaction to be rate-limiting (10), but the question of the energetics and the nature of the transition states in glycolate oxidation remained uncertain. Here, we investigated the reaction mechanism of plant GOX by taking advantage of $^{12}C/^{13}C$ and hydrogen/deuterium isotope effects (Table 2 and 3). Because of the conserved structure and residues involved in the active site of plant (6, 12, 22) and mammalian (9) GOX enzymes, our conclusions concerning the catalytic mechanism (see below) are probably true also for the closely related mammalian enzyme.

In all GOX proteins assayed with [^{2}H]glycolate, we found a rather modest KIE on maximal velocity, $^D\alpha_V$, between 2 and 2.7 (Table 2), suggesting that proton abstraction (k_3) was only partially rate-limiting. In addition, the KIE on effectiveness, $^D\alpha_{V/K}$, was approximately double the $^D\alpha_V$ (values between 3.3 and 4.8). This suggests that glycolate binding itself is also associated with a significant isotope effect (inverse isotope effect on K_m, ≈0.6), meaning that the formation of the Michaelis complex was associated with a strong change in the geometry of glycolate. Alternatively, other reversible steps following substrate binding and prior to glycolate deprotonation may take place (substrate "preprocessing" before the catalytic step, k_3), implying an alteration of the C^α–H force constant. The chemical events responsible for the isotope effect at this hydrogen atom position in such early reaction steps are still to be elucidated. Under the assumption that substrate preprocessing/repositioning occurs during or just after binding, specific residues of the active site are expected to have key roles in determining both K_m and k_{cat} because incomplete preprocessing/repositioning would impede subsequent catalysis. In fact, such residues seem to occur in the GOX active site. In the spinach enzyme, Trp^{108} has been found to be important for both substrate binding and catalysis: when Trp^{108} was replaced by Ser, the enzyme exhibited a very low $K_{m(glycolate)}$ (about 100-fold lower) and very low k_{cat} values with various substrates (glycolate, mandelate, lactate, and 2-hydroxybutyrate) (12). This residue is located in the substrate pocket (close to FMN) and is not conserved in hydroxy-acid oxidases and dehydrogenase flavoproteins. It is believed that amino acids in this position have a side-chain length adapted to the size of the substrate (7, 12) so that substrate binding is adequately tight and associated with possible changes in geometry, thereby facilitating subsequent catalysis (glycolate oxidation). Active site preorganization has been presumed in a similar reaction catalyzed by choline oxidase, consisting in O–H stretching in the α-hydroxyl group to facilitate proton abstraction in subsequent steps (32, 33).

Regardless of the chemical events involved prior to glycolate oxidation itself (k_3), the fact that the latter did not appear to be strictly rate-limiting does not agree with a carbanion-based mechanism, which would have implied a large *V/K* kinetic isotope effect (rate-limiting formation of a dissociative transition state; for reviews, see Refs. 26 and 31). Furthermore, one may take advantage of carbon isotope effects ($^{13}\alpha_V$ and $^{13}\alpha_{V/K}$; Table 3) to compute the commitment factor associated with k_3. Using Equation 8, we found a commitment factor, k_3/k_2, of ≈1.3 and 1.1 with natural and deuterated glycolate, respectively. In other words, the deuterium substitution in C2 had a negligible effect on the kinetic commitment associated with k_3, also indicating that the formation of a carbanion is highly unlikely. It thus appears more plausible that the transition state associated with glycolate oxidation does not imply a substantial change of the C2 geometry (formation of a charged species) but rather involves a concerted bond rearrangement with O2 (hydroxyl) and N5 (FMN). It should also be noted that there was an SIE on k_3, suggesting that exchangeable protons were somehow involved in that chemical step. This effect is more consistent with a hydride transfer mechanism simply because the hydroxyl proton in Tyr residues is exchangeable with the solvent. Exchange rates in Tyr residues buried in enzyme active sites are about 9 s^{-1} (35), that is 3 times slower than the turnover rate. Therefore, during enzymatic assays in D_2O, Tyr residues happened to be only partially deuterated, causing a modest isotope effect. Under the hydride transfer hypothesis, if we assume that about one-third of Tyr residues were deuterated and that the secondary KIE associated with hydrogen/deuterium substitution at Tyr^{129} is near 2, we would expect an SIE of about 1.3, which falls within the observed range. By contrast, under the carbanion hypothesis, no significant solvent isotope effect would be expected on k_3 simply because no Tyr residue primarily participates in bond rearrangements in O2. We nevertheless recognize that other effects may have contributed to the observed SIE such as an effect of solvent viscosity, which is indeed higher in heavy water (36). In fact, recombinant human liver GOX has lower k_{cat} and k_{cat}/K_m values in a more viscous solvent such as glycerol (21). Also, three water molecules have been reported to participate in the catalytic site architecture in recombinant spinach GOX, and their presumed role is to maintain the H-bond network around FMN in the absence of glycolate (6, 37). Therefore, their replacement by D_2O might affect

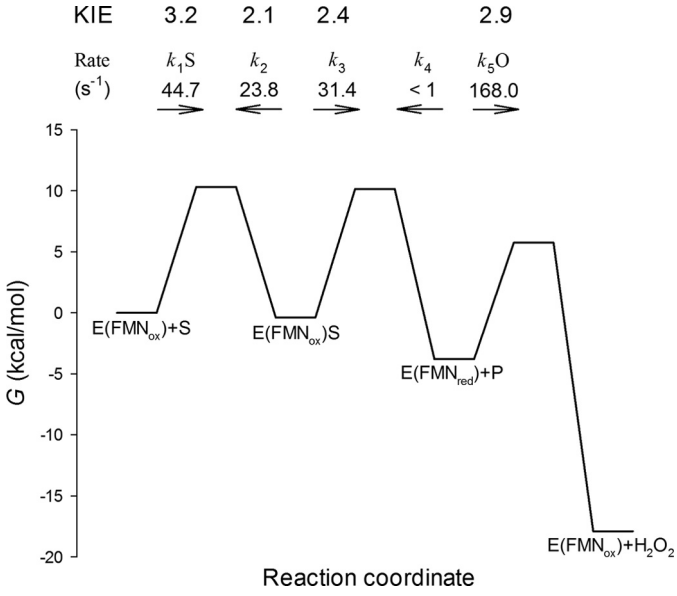

FIGURE 4. **Kinetic energy profile of the GOX-catalyzed reaction.** Intrinsic hydrogen/deuterium KIEs (when [^{2}H$_2$]glycolate is used as a substrate) associated with each elementary step are indicated as well as rate constants (in s^{-1}). For rates that depend upon substrate concentration (k_1S and k_5O), we assumed a value of 0.2 mM. This profile was drawn assuming that the energy barrier associated with k_3 was 10.5 kcal mol^{-1} (see text). *S*, glycolate; *O*, dissolved O_2; *P*, glyoxylate. The overall reaction is shown to be exergonic due to the redox potential E'_0 of glyoxylate/glycolate (−92 mV) and O_2/H_2O_2 (+295 mV) couples.

substrate binding. Here, we observed a tighter glycolate binding (normal SIE on K_m), suggesting that the H-bond network was altered in the presence of D_2O.

Kinetic Energy Profile of the GOX-catalyzed Reaction—To gain insight into the effectiveness of GOX catalysis, we took advantage of the KIE values obtained here to compute commitment factors and therefore generate a kinetic energy profile of the reaction (38). Under the assumption that kinetic constants are given by $k = \kappa k_B T/h \cdot \exp(-\Delta G/RT)$, the ratio of two rate constants k_i and k_{ii} gives the difference in free energy: $RT \cdot \ln(k_i/k_{ii}) = \Delta\Delta G_{ii-i}$. Using our KIE values, the kinetic profile of the reaction was reconstructed with the energy barrier of one step fixed at a certain value (for a recent similar example on Rubisco, see Ref. 39). The effective free energy barrier of the turnover rate ($k_{cat} = k_3$) is assumed to be 44 kJ mol^{-1} (10.5 kcal mol^{-1}) considering the apparent activation energy (E_a) on GOX velocity (using data obtained at different temperatures (20, 40)). This value is in agreement with E_a values obtained for similar enzymes: 46 kJ mol^{-1} for lactate oxidase (the ancestor of GOX (2)) and 56 kJ mol^{-1} for D-amino-acid oxidase (41, 42). The k_3 itself corresponds here to the turnover rate at saturating glycolate and was found to be near 31 s^{-1}. It should be noted that we assumed glycolate reprotonation (reverse reaction) to be negligible ($k_4 \approx 0$). In fact, enzyme catalysis proceeds forward (FMN reduction by glycolate) even in the absence of dissolved O_2, indicating that glycolate oxidation is irreversible (10). As stated above, the $^{12}C/^{13}C$ KIE indicated that the commitment factor k_3/k_2 was near 1.3, and thus k_2 was about 23 s^{-1} (Fig. 4). Using this value and K_m allowed us to compute k_1S (where *S* is glycolate concentration), which was found to be near 44 s^{-1} at 0.2 mM glycolate (physiological concentration). Thus, no specific step of the reductive half-reaction appeared to be rate-limiting because rates were all within the same order of magnitude. By contrast, the oxidative half-reaction appeared to be rapid because $k_3/k_5[O_2]$ was about 0.1–0.2 (Table 1). In other words, the reductive half-reaction was limiting when compared with the oxidative half-reaction, but no specific step within the reductive half-reaction was strictly rate-limiting. Unsurprisingly therefore, there was no large difference in energy barriers along the reductive half-reaction. The overall reaction was driven by the free enthalpy drawdown (redox equilibrium at physiological concentrations) (Fig. 4).

Intrinsic isotope effects associated with each elementary step were found to be within the 2.0–3.2 range with no step that fractionated highly against ^{2}H (KIE of 4 or above) (Fig. 4). Because in hydrogen transfer events KIE is expected to be maximal when the transition state is symmetrical (for a practical example on formate dehydrogenase, see Ref. 43), the KIE on k_3 observed here (2.4) rather suggests a late transition state associated with glycolate deprotonation. Accordingly, the relatively high intrinsic $^{12}C/^{13}C$ isotope effect of about 1.045 suggests that deprotonation is not the sole chemical event occurring in step k_3 because a simple C–H bond stretching (wave number, ≈3000 cm^{-1}) is expected to be associated with an intrinsic KIE of about 1.025. A simultaneous rearrangement of the hydroxyl group (to a C=O bond) and hydrogen abstraction in the transition state, indicative of a concerted hydride transfer, is thus likely. Rather similar situations with the same order of magnitude for the carbon isotope effect (≈1.040) involving similar chemical rearrangements (carbonyl formation along hydride transfer at C1 in the glucose dehydrogenase (44) or formate dehydrogenase (45) reactions) have been found. We nevertheless recognize that in Fig. 4 the formation of a late transition state is not associated with a high energy barrier. In this figure, the profile was reconstructed using the apparent energy barrier associated with k_3 (temperature-response curves reported in the literature; see above), and this should be examined further in future studies. Uncertainty also remains as to whether the reaction proceeds via a hydrogen tunneling as found in the similar reaction of choline oxidase (see Ref. 33) and suggested by the irreversibility of glycolate deprotonation. Future studies are thus warranted to explore the temperature response of $^1H/^2H$ KIE and the value of Eyring pre-exponential factors to determine whether the transition state is classical or consistent with hydride ion tunneling.

In conclusion, by measuring kinetic isotope effects, it is shown that the short-chain α-hydroxy-acid oxidase GOX reaction mechanism involves a hydride transfer mechanism, thereby strengthening the idea that this mechanism is common to α-hydroxy-acid oxidase family members. Interesting, the analysis of our data suggested that glycolate deprotonation was only partially rate-limiting and that the formation of the substrate-enzyme complex was also an important limiting factor. Such data could be useful to help design drugs and/or herbicides. Indeed, our KIE values could be applied to compute steric and electronic maps for the transition state of the GOX reaction (46). This would allow the synthesis of stable transition state analogs that are powerful enzymatic inhibitors. Inhibition of GOX has been considered as a possible treatment for several

oxalate-mediated diseases in humans such as hyperoxaluria and renal lithiasis (47) and in plants as a target for herbicide action (48). Mutants of photorespiratory enzymes are non-viable in air, exhibiting severely stunted growth and chlorotic leaves (*e.g.* Ref. 49). This has been seen for the *go1* (GOX) mutant of *Z. mays* (17). In the case of plant photorespiratory GOX, because of the similarity in enzymatic parameters, KIE values, and reaction mechanism of both C_3 and C_4 plant enzymes, a transition state analog herbicide would not be selective (that is, it would not be possible to design a specific herbicide to eliminate C_3 weeds only in a maize field), but it could rather be used as a general weed killer. Interestingly, the introduction of a photorespiratory glycolate bypass in the chloroplast by the expression of several transgenes (50, 51) has led to increases in *Arabidopsis* biomass (see Ref. 50) and potato tuber yield (51). By inhibiting GOX activity in such plants, it might be possible to further improve the observed transgenic effects on yield by increasing the flux through the bypass.

Furthermore, stable carbon isotopes at natural abundance have been used over the years to examine physiological, ecological, and geochemical processes. It is possible to exploit $\delta^{13}C$ in metabolites to calculate metabolic fluxes; however, to undertake such an approach, it is crucial to know the isotopic fractionation of each enzymatic reaction during a given biochemical and biophysical process (see Ref. 52 and references therein). The fact that *in vitro* plant GOX activity leads to an isotopic discrimination at natural abundance as observed in this work (Table 3) means that the $\delta^{13}C$ of glycolate (and/or glyoxylate) of leaf extracts could be tested to calculate *in planta* photorespiratory fluxes.

Acknowledgments—We are very thankful to Elementar France and Agilent Technologies for loan of the Liquiface and the HPLC, respectively. We thank the Plateforme d'Analyse Proteomique de Paris Sud-Ouest (Unité Mixte de Recherche de Génétique Végétale, Ferme du Moulon, Gif sur Yvette, France) for mass spectroscopy analysis of the recombinant proteins.

REFERENCES

1. Diêp Lê, K. H., and Lederer, F. (1991) Amino acid sequence of long chain α-hydroxy acid oxidase from rat kidney: a member of the family of FMN-dependent α-hydroxy acid-oxidizing enzymes. *J. Biol. Chem.* **266,** 20877–20881
2. Esser, C., Kuhn, A., Groth, G., Lercher, M. J., and Maurino, V. G. (2014) Plant and animal glycolate oxidases have a common eukaryotic ancestor and convergently duplicated to evolve long-chain 2-hydroxy acid oxidases. *Mol. Biol. Evol.* **31,** 1089–1101
3. Richardson, K. E., and Tolbert, N. E. (1961) Oxidation of glyoxylic acid to oxalic acid by glycolic acid oxidase. *J. Biol. Chem.* **236,** 1280–1284
4. Williams, H. E., and Smith L. H., Jr. (1968) Disorders of oxalate metabolism. *Am. J. Med.* **45,** 715–735
5. Friend, A. D. (2010) Terrestrial plant production and climate change. *J. Exp. Bot.* **61,** 1293–1309
6. Lindqvist, Y., and Brändén, C. I. (1989) The active site of spinach glycolate oxidase. *J. Biol. Chem.* **264,** 3624–3628
7. Tsai, C.-L., Gokulan, K., Sobrado, P., Sacchettini, J. C., and Fitzpatrick, P. F. (2007) Mechanistic and structural studies of H373Q flavocytochrome b_2: effects of mutating the active site base. *Biochemistry* **46,** 7844–7851
8. Müh, U., Williams, C. H., Jr., and Massey, V. (1994) Lactate monooxygenase: site-directed mutagenesis of the postulated active site base histidine 290. *J. Biol. Chem.* **269,** 7989–7993
9. Bourhis, J. M., Vignaud, C., Pietrancosta, N., Guéritte, F., Guénard, D., Lederer, F., and Lindqvist, Y. (2009) Structure of human glycolate oxidase in complex with the inhibitor 4-carboxy-5-[(4-chlorophenyl)-sulfanyl]-1.2.3-thiadiazole. *Acta Crystallogr. Sect. F Struct. Biol. Cryst. Commun.* **65,** 1246–1253
10. Macheroux, P., Massey, V., Thiele, D. J., and Volokita, M. (1991) Expression of spinach glycolate oxydase in *Saccharomyces cerevisiae*: purification and characterization. *Biochemistry* **30,** 4612–4619
11. Pennati, A., and Gadda, G. (2011) Stabilization of an intermediate in the oxidative half-reaction of human liver glycolate oxidase. *Biochemistry* **50,** 1–3
12. Stenberg, K., Clausen, T., Lindqvist, Y., and Macheroux, P. (1995) Involvement of Tyr24 and Trpl08 in substrate binding and substrate specificity of glycolate oxidase. *Eur. J. Biochem.* **228,** 408–416
13. Nishimura, M., Akhmedov, Y. D., Strzalka, K., and Akazawa, T. (1983) Purification and characterization of glycolate oxidase from pumpkin cotyledons. *Arch. Biochem. Biophys.* **222,** 397–402
14. Devi, M. T., Rajagopalan, A. V., and Raghavendara, A. S. (1996) Purification and properties of glycolate oxydase from plants with different photosynthetic pathways: distinctness of C4 species from that of a C3 specie and a C3-C4 intermediate. *Photosynth. Res.* **47,** 231–238
15. Popov, V. N., Dmitrieva, E. A., Eprintsev, A. T., and Igamberdiev, A. U. (2003) Glycolate oxidase isoforms are distributed between the bundle sheath and mesophyll tissues of maize leaves. *J. Plant Physiol.* **160,** 851–857
16. Hackenberg, C., Kern, R., Hüge, J., Stal, L. J., Tsuji, Y., Kopka, J., Shiraiwa, Y., Bauwe, H., and Hagemann, M. (2011) Cyanobacterial lactate oxidases serve as essential partners in N_2 fixation and evolved into photorespiratory glycolate oxidases in plants. *Plant Cell* **23,** 2978–2990
17. Zelitch, I., Schultes, N. P., Peterson, R. B., Brown, P., and Brutnell, T. P. (2009) High glycolate oxidase activity is required for survival of maize in normal air. *Plant Physiol.* **149,** 195–204
18. Jossier, M., Bouly, J.-P., Meimoun, P., Arjmand, A., Lessard, P., Hawley S., Grahame Hardie, D., and Thomas, M. (2009) SnRK1 (SNF1-related kinase 1) has a central role in sugar and ABA signalling in *Arabidopsis thaliana*. *Plant J.* **59,** 316–328
19. Laemmli, U. K. (1970) Cleavage of structural proteins during the assembly of the head of bacteriophage T4. *Nature* **227,** 680–685
20. Vignaud, C., Pietrancosta, N., Williams, E. L., Rumsby, G., and Lederer, F. (2007) Purification and characterization of recombinant human liver glycolate oxidase. *Arch. Biochem. Biophys.* **465,** 410–416
21. Pennati, A., and Gadda, G. (2009) Involvement of ionizable groups in catalysis of human liver glycolate oxidase. *J. Biol. Chem.* **284,** 31214–31222
22. Fitzpatrick, P. F. (2007) Insights into the mechanisms of flavoprotein oxidases from kinetic isotope effects. *J. Labelled Comp. Radiopharm.* **50,** 1016–1025
23. Kurtz, K. A., Rishavy, M. A., Cleland, W. W., and Fitzpatrick, P. F. (2000) Nitrogen isotope effects as probes of the mechanism of D-amino acid oxidase. *J. Am. Chem. Soc.* **122,** 12896–12897
24. Ralph, E. C., Anderson, M. A., Cleland, W. W., and Fitzpatrick, P. F. (2006) Mechanistic studies of the flavoenzyme tryptophan 2-monooxygenase: deuterium and ^{15}N kinetic isotope effects on alanine oxidation by an L-amino acid oxidase. *Biochemistry* **45,** 15844–15852
25. Furuichi, M., Suzuki, N., Dhakshnamoorhty, B., Minagawa, H., Yamagishi, R., Watanabe, Y., Goto, Y., Kaneko, H., Yoshida, Y., Yagi, H., Waga, I., Kumar, P. K., and Mizuno, H. (2008) X-ray structures of *Aerococcus viridians* lactate oxidase and its complex with D-lactate at pH 4.5 show an α-hydroxy acid oxidation mechanism. *J. Mol. Biol.* **378,** 436–446
26. Macheroux, P., Kieweg, V., Massey, V., Söderlind, E., Stenberg, K., and Lindqvist, Y. (1993) Role of tyrosine 129 in the active site of spinach glycolate oxidase. *Eur. J. Biochem.* **213,** 1047–1054
27. Ortega-Galisteo, A. P., Rodríguez-Serrano, M., Pazmiño, D. M., Gupta, D. K., Sandalio, L. M., and Romero-Puertas, M. C. (2012) S-Nitrosylated proteins in pea (*Pisum sativum* L.) leaf peroxisomes: changes under abiotic stress. *J. Exp. Bot.* **63,** 2089–2103
28. Hodges, M., Jossier, M., Boex-Fontvieille, E., and Tcherkez, G. (2013) Protein phosphorylation and photorespiration. *Plant Biol.* **15,** 694–706
29. Quaye, O., Lountos, G. T., Fan, F., Orville, A. M., and Gadda, G. (2008)

Role of Glu312 in binding and positioning of the substrate for the hydride transfer reaction in choline oxidase. *Biochemistry* **47,** 243–256
30. Gadda, G. (2008) Hydride transfer made easy in the reaction of alcohol oxidation catalyzed by flavin-dependent oxidases. *Biochemistry* **47,** 13745–13753
31. Cleland, W. W. (2005) The use of isotope effects to determine enzyme mechanisms. *Arch. Biochem. Biophys.* **433,** 2–12
32. Ralph, E. C., Hirschi, J. S., Anderson, M. A., Cleland, W. W., Singleton, D. A., and Fitzpatrick, P. F. (2007) Insights into the mechanism of flavoprotein-catalyzed amino oxidation from nitrogen isotope effects on the reaction of *N*-methyltryptophan oxidase. *Biochemistry* **46,** 7655–7664
33. Sobrado, P., Daubner, S. C., and Fitzpatrick, P. F. (2001) Probing the relative timing of hydrogen abstraction steps in the flavocytochrome b_2 reaction with primary and solvent deuterium isotope effects and mutant enzymes. *Biochemistry* **40,** 994–1001
34. Sobrado, P., and Fitzpatrick, P. F. (2003) Solvent and primary deuterium isotope effects show that lactate CH and OH bond cleavages are concerted in Y254F flavocytochrome b_2, consistent with a hybrid transfer mechanism. *Biochemistry* **42,** 15208–15214
35. Takeda, M., Jee, J., Ono, A. M., Terauchi, T., Kainosho, M. (2009) Hydrogen exchange rate of tyrosine hydroxyl groups in proteins as studied by the deuterium isotope effect on C_ζ chemical shifts. *J. Am. Chem. Soc.* **131,** 18556–18562
36. Hardy, R. C., and Cottington, R. L. (1949) Viscosity of deuterium oxide and water in the range 5° to 125° C. *J. Res. Natl. Bur. Stand.* **42,** 573–578
37. Stenberg, K., and Lindqvist, Y. (1997) Three-dimensional structures of glycolate oxidase with bound active-site inhibitors. *Protein Sci.* **6,** 1009–1015
38. Albery, W. J., and Knowles, J. R. (1976) Free-energy profile of the reaction catalyzed by triosephosphate isomerase. *Biochemistry* **15,** 5627–5631
39. Tcherkez, G. G., Bathellier, C., Stuart-Williams, H., Whitney, S., Gout, E., Bligny, R., Badger, M., and Farquhar G. D. (2013) D_2O solvent isotope effects suggest uniform energy barriers in ribulose-1,5-bisphosphate carboxylase/oxygenase catalysis. *Biochemistry* **52,** 869–877
40. Rocha, M. J., Rocha, E., Resende, A. D., and Lobo-da-Cunha, A. (2003) Measurement of peroxisomal enzyme activities in the liver of brown trout (*Salmo trutta*), using spectrophotometric methods. *BMC Biochem.* **4,** 2
41. Ghisla, S., and Massey, V. (1977) Studies on the mechanism of action of the flavoenzyme lactate oxidase. Proton uptake and release during the binding of transition state analogs. *J. Biol. Chem.* **252,** 6729–6735
42. Pollegioni, L., Blodig, W., and Ghisla, S. (1997) On the mechanism of D-amino acid oxidase: structure/linear free energy correlations and deuterium kinetic isotope effects using substituted phenylglycines. *J. Biol. Chem.* **272,** 4924–4934
43. Scharschmidt, M., Fisher, M. A., and Cleland, W. W. (1984) Variation of transition-state structure as a function of the nucleotide in reactions catalyzed by dehydrogenases. 1. Liver alcohol dehydrogenase with benzyl alcohol and yeast aldehyde dehydrogenase with benzaldehyde. *Biochemistry* **23,** 5471–5478
44. Rendina, A. R., Hermes, J. D., and Cleland, W. W. (1984) Use of multiple isotope effects to study the mechanism of 6-phosphogluconate dehydrogenase. *Biochemistry* **23,** 6257–6262
45. Hermes, J. D., Morrical, S. W., O'Leary, M. H., and Cleland, W. W. (1984) Variation of transition-state structure as a function of the nucleotide in reactions catalyzed by dehydrogenases. 2. Formate dehydrogenase. *Biochemistry* **23,** 5479–5488
46. Gluza, K., and Kafarski, P. (2013) in *Drug Discovery* (El-Shemy, H. A., ed) pp. 325–372, InTech, 10.5772/52504
47. Williams, H. W., Eichler, E., Randall, W. C., Rooney, C. S., Cragoe, E. J., Jr., Streeter, K. B., Schwam, H., Michelson, S. R., Patchett, A. A., and Taub, D. (1983) Inhibitors of glycolic acid oxidase. 4-Substituted 2,4-dioxobutanoic acid derivatives. *J. Med. Chem.* **26,** 1196–1200
48. Fendrich, G., and Ghisla, S. (1982) Studies of glycollate oxidase from pea leaves. Determination of stereospecificity and mode of inhibition by α-hydroxybutynoate. *Biochim. Biophys. Acta* **702,** 242–248
49. Timm, S., Mielewczik, M., Florian, A., Frankenbach, S., Dreissen, A., Hocken, N., Fernie, A. R., Walter, A., and Bauwe, H. (2012) High-to-low CO_2 acclimation reveals plasticity of the photorespiratory pathway and indicates regulatory links to cellular metabolism of *Arabidopsis*. *PLoS One* **7,** e42809
50. Peterhansel, C., Krause, K., Braun, H. P., Espie, G. S., Fernie, A. R., Hanson, D. T., Keech, O., Maurino, V. G., Mielewczik, M., and Sage, R. F. (2013) Engineering photorespiration: current state and future possibilities. *Plant Biol.* **15,** 754–758
51. Nölke, G., Houdelet, M., Kreuzaler, F., Peterhänsel, C., and Schillberg, S. (2014) The expression of a recombinant glycolate dehydrogenase polyprotein in potato (*Solanum tuberosum*) plastids strongly enhances photosynthesis and tuber yield. *Plant Biotechnol. J.* **12,** 734–742
52. Tcherkez, G., Mahé, A., and Hodges, M. (2011) $^{12}C/^{13}C$ fractionations and plant metabolism. *Trends Plant Sci.* **16,** 499–506

Enzymology:

Experimental Evidence for a Hydride Transfer Mechanism in Plant Glycolate Oxidase Catalysis

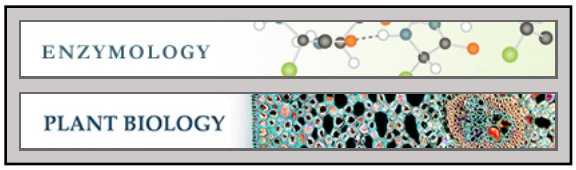

Younès Dellero, Caroline Mauve, Edouard Boex-Fontvieille, Valérie Flesch, Mathieu Jossier, Guillaume Tcherkez and Michael Hodges

J. Biol. Chem. 2015, 290:1689-1698.
doi: 10.1074/jbc.M114.618629 originally published online November 21, 2014
